Colloids and Surfaces A: Physicochemical and Engineering Aspects 682 (2024) 132837

Contents lists available at ScienceDirect

Colloids and Surfaces A: Physicochemical and Engineering Aspects

journal homepage: www.elsevier.com/locate/colsurfa

Jettability and printability of customized gold nanoparticles-based ink on flexible substrate through inkjet printing process

Mohammed Shariq [a], Rebeka Rudolf [b,c], Peter Majerič [b,c], Somnath Chattopadhyaya [d], Rupert Kargl [e,f], Bernd Friedrich [g], Andrews Nirmala Grace [a], Amit Rai Dixit [d,*]

[a] Centre for Nanotechnology Research, VIT University, Vellore, Tamil Nadu 632014, India
[b] Faculty of Mechanical Engineering, University of Maribor, Maribor 2000, Slovenia
[c] Zlatarna Celje d.o.o., Celje 3000, Slovenia
[d] Department of Mechanical Engineering, IIT(ISM) Dhanbad, Jharkhand 826004, India
[e] Institute of Chemistry and Technology of Biobased Systems, Graz University of Technology, 8010 Graz, Austria
[f] Laboratory for Characterization and Processing of Polymers, University of Maribor, 2000 Maribor, Slovenia
[g] IME Institute of Metal Processing and Metal Recycling, RWTH Aachen, 52056, Germany

GRAPHICAL ABSTRACT

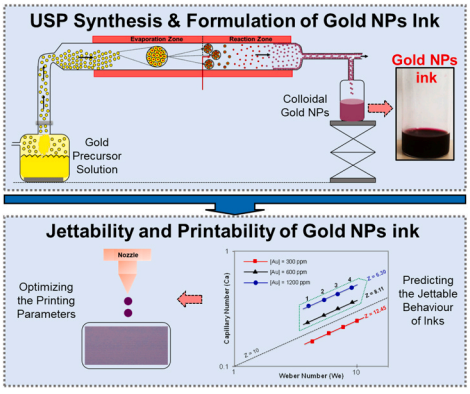

ARTICLE INFO

Keywords:
Gold nanoparticles
Inkjet based inks
Additive manufacturing
Jettability window
Printability
Flexible substrate

ABSTRACT

Among the different metal nanoparticles for formulating inkjet-based conductive inks, gold remains the best choice for fabricating different patterns on economical and bio-degradable substrates such as commercial photo papers for developing low-cost sensing devices. Formulating customized gold nanoparticle (AuNPs) inks remains challenging as the ink must meet specific physical, chemical and rheological properties to achieve appropriate jettable behaviour and printable characteristics. It should exhibit well-controlled viscoelastic response for the smooth and optimized flow through the nozzles and then cure immediately to facilitate the shape retention of deposited feature. In this work, the jettability window definition framework using dimensionless numbers such as Re, We, Ca, and Z are defined for the aqueous-based AuNPs inks synthesized via ultrasonic spray pyrolysis technique and formulated into three concentration levels of 300, 600, and 1200 ppm. A theoretical CFD based

* Corresponding author.
E-mail address: amitraidixit@iitism.ac.in (A.R. Dixit).

https://doi.org/10.1016/j.colsurfa.2023.132837
Received 25 August 2023; Received in revised form 12 November 2023; Accepted 19 November 2023
Available online 23 November 2023

simulation study is conducted to observe the ink droplet formation behaviour at different droplet velocities through inkjet nozzle. Among these formulated inks, 1200 ppm shows the most favourable behaviour as obtained through the simulation and jettability window results. It is tested further to see how different printing settings, like pulse voltage and number of repetitions, affected the continuity and density of the ink, affecting the quality of the printed AuNPs. This work demonstrates the process capabilities of inkjet printing technology by testing the formulated AuNPs ink.

1. Introduction

Nowadays, inkjet printing (IJP) is among the most attractive choices for a material jetting technique because of its simple, economical, and high-production capabilities. It comprises the material deposition on different substrates through the customized functional inks of metal NPs. It allows the printing of contour-shaped patterns and gives enormous flexibility in printing other functional inks. Inkjet printing of NPs ink offers unique advantages compared to traditional methods like template-assisted assembly and laser printing as listed in Table 1**.** This cutting-edge technique leverages the precision and versatility of inkjet technology to precisely deposit nanoparticles onto substrates, enabling tailored and controlled assembly at the nanoscale.In drop-on-demand (DoD) based IJP [1], ink droplets are formed using various methods such as thermal [2], piezoelectric [3], acoustic [4], electrostatic [5], electrohydrodynamic [5], and valve methods [6]. These methods involve generating a pressure pulse wave to create the droplets. The first two methods gained success in the industrial utilization of IJP. In the thermal-based DoD printer, the customized ink is heated rapidly to a high temperature, which creates a bubble at the surface of a heater, causing a pressure pulse that extrudes ink droplets through the nozzle. The vapour bubble collapses as the ink droplets are ejected, thereby generating a force to refill the ink. However, the high temperature during the thermal-based IJP can affect the functional properties of the formulated NPs ink [7].

In a piezoelectric-based DoD printer [8], as shown in Fig. 1, the ink droplets are created by the expansion and contraction of the piezoelectric transducer when an electric field is applied. A positive voltage is applied to this crystal during the time interval, which causes an expansion generating a pressure wave of ink in the nozzle chamber. This voltage is continuously maintained for the dwell time duration, allowing the propagation of the generated pressure wave throughout the chamber. After that, the magnitude of the voltage decreases in the time fall duration, resulting in the contraction and subsequently in the ejection of the ink's droplet. The nozzle remains contracted and minimizes the satellite formation as it cancels out generated pressures [9]. The NPs inks are mostly thermally sensitive, and high temperatures can cause aggregation and changes in the functional properties [10]. Therefore, the piezoelectric-based DoD inkjet printers were best suited for these customized inks as they offer printing with minimal waste and overall costs. Its availability from low-cost office-based printers to high-end R&D-based printers will provide more flexibility to fabricate sensing and diagnostic devices in any part of the globe [11].

AuNPs ink achieves an important place and position in developing sensing devices, diagnostics, catalysts and wearables through different industrially up-scaled processes [13,14]. These concentrated inks are highly promising due to their excellent physical, chemical and biocompatibility properties [15,16]. One of the widely explored applications for AuNPs is the fabrication of nano-metallic-based sensors on different substrates such as colourimetric, surface plasmon resonance, bio-sensors, and gas, electrical, and electrochemical sensing applications [17–19]. AuNPs-based printed patterns are used as the colourimetric sensors and provide an alternative detection system of impurities of heavy metal ions of Hg^{+}, Co^{2+}, Mn^{2+}, Pb^{2+}, Ca^{2+}, and Cd^{2+} in the drinking groundwater [20]. It is because of the excellent biocompatibility and unique optoelectronic properties. Using IJP to create patterns of AuNPs on paper substrates, taking advantage of their photothermal properties, has opened up possibilities for developing affordable diagnostic devices. These devices can detect various biomarkers, including glucose [21] and other biomarkers [22].

AuNPs encapsulated with Prussian blue analogues (PBA) are utilized to develop security labels with multiple label information by IJP technique. The AuNPs are synthesized using the seed growth method with a size distribution of 60 nm. These inks were tested with Raman spectroscopy to obtain an identifiable and stable SERS signal [30]. One step fabrication of gold films by reactive inkjet printing is also gaining importance for fast production. In this approach, a metal salt of gold is printed and thereafter a second ink containing a reducing agent (e.g. $NABH_4$ or anti-oxidants) that requires the Au^{3+} ion into Au^{0} ions. It eliminates the multiple steps of the wet chemistry and washing involved in ink formulation. This process involves the chemical reactions that occur after deposition. Controlling the reaction kinetics to occur it uniformly across the printed pattern can be challenging [31].

The AuNPs are utilized because of their high surface-to-volume ratio. It helps in the high-density biochemical interaction of these NPs and increases the high-sensitivity analysis of the printed sensors [32]. The ability for patients to test themselves for a range of conditions within the comfort of their homes is desirable. The point of care (PoC) diagnostic device market is poised to reach $27.5 million by 2018, with a wide range of PoC technologies covering many different diseases and conditions. To ensure the commercial viability of these technologies, there is a requirement for low-cost, high-yield fabrication of such devices [33]. The use of AuNPs inks through IJP techniques is an obvious step towards mass production of these devices at a relatively low cost compared to the semi-conductor cleanroom techniques, which involve multiple processing steps using complex and expensive facilities. However, the critical factor is the formulation with optimum rheological properties of these inks for making different patterns on low-cost substrates. The IJP of spherically shaped AuNPs with a size diameter of less than 50 nm on the paper substrates is much focus for fabricating these diagnostic tools [34]. Their production requires inexpensive, easily scalable, and one-time usable devices ideally suited to the IJP process. In these customized formulated AuNPs inks, the surface tension (ST), viscosity, and concentration are the critical physical properties that govern the formation of stable droplets from the nozzle of the cartridge of inkjet printers [35]. Therefore, these ink properties and the nozzle's diameter strongly influence the droplet formation of the AuNPs ink. The printing performance of these formulated inkjet inks can be evaluated by carefully analyzing the jetting behaviour onto the target location of the substrate [36]. The successful jetting of these inks through the nozzle of the printer results in the formation of single droplets. Successful jettable inks are formulated by optimizing the ink's different physiochemical, rheological, flow and wetting properties. These properties must be carefully optimized while designing the ink formulation [37]. The jettability windows are used to calculate and define the jetting performance with the help of the four primary dimensionless numbers: Reynold (Re), Weber (We), Capillary (Ca), and Fromm (Z) number(s) [38]. In the Fig. 2**,** the terms ρ, μ and γ are the density, viscosity and ST of the ink fluid respectively, d is the diameter of the printer nozzle and v is the velocity of the ink droplet. The Capillary number (Ca) is defined as the ratio of viscous to surface tension forces, Weber (We) number is the ratio of inertial to surface tension forces and Reynold number (Re) is the ratio of inertial to viscous forces.

Fromm number (Z) is defined as the ratio of inertial with surface

Table 1
Comparison of inkjet printing with template assisted assembly and laser printing with working principle, material compatibility, advantages and challenges.

Technique	Working Principle	Material Compatibility	Advantages	Challenges	Ref.
Template assisted Assembly	It uses a template or substrate with predefined patterns or structures to guide the assembly of nanoparticles	The choice of template and NPs materials can influence the compatibility and success of the assembly. Compatibility issues may arise when dealing with certain materials.	• High precision and control over the placement of nanoparticles. • The template guides the nanoparticles into specific locations, allowing for well-defined structures. • It is well-suited for creating ordered arrays and structures with specific geometries. However, it may be less versatile for creating more arbitrary patterns.	• The throughput depends on the template and assembly method. It can be time-consuming for large-scale production. • It is often used for applications where ordered nanoparticle arrays or precise structures are required, such as in electronics, optics, and sensors.	[23–25]
Inkjet Printing	It employs a printhead that ejects tiny droplets of liquid ink onto the paper or other surfaces to create text and images. The ink droplets are deposited in a pattern that forms the desired content	compatible with a variety of nanoparticle inks, but it may have limitations in handling highly concentrated or viscous inks due to printhead clogging.	• It provides the non-contact and mask less deposition of the NPs with multi material flexibility • It can be used to create a wide range of patterns and designs, making it suitable for both regular and irregular structures with high resolution. • It is generally faster and more scalable for high-throughput applications, making it suitable for mass production • It is used in a variety of fields, including electronics, flexible electronics, photovoltaics, biosensors, and 3D printing, due to its versatility and scalability.	• Requires a precise control of rheological properties • Nozzle plate flooding, clogging and irregular droplet ejection	[26,27]
Laser based Printing	It utilizes a laser to selectively heat and evaporate a carrier solvent in a nanoparticle ink, leaving behind the nanoparticles on the substrate.	are generally versatile and can work with a wide range of nanoparticle inks, including metallic, organic, and inorganic materials	• Fast and suitable for high-throughput production, especially for small feature sizes.	• It can be more complex and costly, requiring precise optics and control systems • Final obtained surface consists of powdery impurities • Limited material flexibility	[28,29]

(*continued on next page*)

Table 1 (*continued*)

Technique	Working Principle	Material Compatibility	Advantages	Challenges	Ref.
			• It can achieve higher resolution and precision in nanoparticle ink deposition. It allows for finer control over the placement of nanoparticles, resulting in more intricate and detailed patterns. • It can reduce the risk of nanoparticle agglomeration, as they do not rely on mechanical pressure or thermal effects that can cause particles to clump together.	• Degradation of photosensitive material leading to poor performance under load	

tension to viscous forces. It is the reciprocal of Ohnesorge number. Among these four dimensionless numbers, Z number is used for defining the jettability of the metal NPs based inks because it correlates all the three forces of the fluid ink: viscous, inertial and ST forces while the Re, We, and Ca number balances two forces against each other. In the reported literature, the most appropriate jettable range of Z number is $1 \leq Z \leq 10$ for AuNPs inks or fluids with a similar range of rheological properties [39].

In this work, the formulated aqueous AuNPs inks in three concentration levels of 300, 600, and 1200 ppm through the USP method, as reported in our previous work [40,41] are evaluated to determine the jettability and printability characteristics on the flexible photo paper substrate by utilizing the IJP technology. Initially, the jettability window characterized by Ca-We and We-Z numbers are developed for these inks. Considering the jettability window defined by these numbers, the ST force will be the normalizing force for Ca-We, while the inertial force is in the case of the We-Z window. Plotting these windows will provide the most helpful and insightful knowledge regarding jettability and helps to identify the most favourable concentration for the IJP process [42]. The theoretical CFD simulation study is also incorporated to observe the ink droplet formation behaviour at different droplet velocities through a DoD inkjet nozzle. Finally, the most favourable ink is tested for the printability characteristics, such as the morphology and the density of the printed AuNPs achieved through the inkjet printing technique. The surface morphology of printed patterns with different repetitions is characterized by the SEM-EDX technique. The process parameter, such as pulse actuation voltage, is controlled and optimized to improve printing characteristics, such as the continuity and density of the AuNPs on the printed patterns. The rheological properties of AuNPs ink are taken from our last published article [43] as mentioned in Table 2**.**

2. Materials and Methods

2.1. AuNPs Synthesis and Ink Formulation

AuNPs are synthesized through the USP **(**Fig. 3**a)** method by utilizing the varying concentration of aqueous-based Au (III) acetate (Au $(CH_3COO)_3$) precursor solution. It is carried out on the modular USP device at the IME Institute of Process Metallurgy and Metal Recycling, RWTH Aachen, Germany. An aqueous solution of $Au(CH_3COO)_3$ acetate with HCl and NaOH is used as the precursor solution. This modular USP device is redesigned with a modular separate heating zone in order to divide the aerosol droplet evaporation and particle drying from the rest of synthesis stages. The precursor solution is atomized with an ultrasonic aerosol generator (Gapusol, RBI France with piezoelectric transducer membrane frequency of 1.6 MHz using intensity to 9). After the atomization, the droplets are carried to the first heated zone of the reactor which consisted of a quartz tube (length = 28 cm and diameter = 2 cm) and the temperature of the first heating zone temperature is kept at 100 °C in the experiment **(**Table 3**)** while the second heating zone with the same length and diameter continuously maintained at 300 °C. Dry Nitrogen (N_2, 99.9%) is used as a carrier gas with a flow rate of 2–1 l/min where they begin to evaporate and shrink. This shrinkage and dehydration of the water content from the solute particles of gold precursor increases the concentration of Au inside the evaporated droplet. Hydrogen gas used for the reduction of the aerosol droplets of the precursor solution into AuNPs is directly fed into the Chamber-II at a flow rate of 1–0.5 l/min. It provides the sufficient reduction energy for the dried aerosol particles containing Au^{3+} ions to be converted into pure AuNPs The synthesized dark red coloured AuNPs are collected in the glass bottles containing 500 ml of de-ionized (DI) water mixed with the 0.1 wt% of PVP40. A detailed description of the complete process is mentioned in the reference [44]. The collected AuNPs in colloidal suspension form are formulated in three different ink concentrations of 300, 600, and 1200 ppm through rota-vaporization, centrifugation, and filtration process, as shown in Fig. 3**b).** Rota-vapour technology helps in concentrating the synthesized AuNPs from USP to remove the DI water solvent without heating it to the boiling temperature. After rota-vaporization, the AuNPs were further concentrated by centrifuging them with the help of AMICON Ultra-15 membrane filters (100,000 NMWL) **(**Fig. 3**c).** These membrane filter also helps in removing any impurities present in the AuNPs. The centrifuged concentrated AuNPs were further filtered through a 450 nm syringe filter to remove any aggregates formed during the process. The membrane filters are chosen with specific pore sizes accordingly to the NPs size distribution. This

allows for the selective removal of impurities based on their particle size. This is particularly useful for eliminating larger contaminants that may be present in the AuNPs based ink, such as aggregates, or larger particulate matter. It provides a consistent and precise method for removing impurities from AuNPs inks [45]. It can also be easily scaled up for large-volume ink purification processes which is crucial for industrial applications, where significant quantities of ink may need to be purified efficiently and consistently.

2.2. Modelling of the AuNPs ink droplet formation of 1200 ppm

2.2.1. Assumptions

- The fluid flow domain is large enough that the continuum assumption is valid.
- The synthesized AuNPs ink is assumed to be Newtonian fluid and incompressible. Hence, the Navier-Stokes equation is also valid in this case.
- The effect of gravity is neglected in this domain.
- It is assumed that the ink in contact with the diaphragm below the piezo material moves with the same velocity as the latter.

2.2.2. Governing equations

The main governing equations for the motion of the fluid (AuNPs ink) are: -

- The continuity equation is

$$\frac{\partial \rho}{\partial t} + \nabla.(\rho \vec{v}) = 0 \tag{1}$$

- For 2D-axisymmetric flow,

$$\frac{\partial \rho}{\partial t} + \frac{\partial}{\partial x}(\rho v_x) + \frac{\partial}{\partial r}(\rho v_r) + \frac{\rho v_r}{r} = 0 \tag{2}$$

- The momentum equation is given by

$$\frac{\partial}{\partial t}(\rho \vec{v}) + \nabla.(\rho \vec{v}\vec{v}) = -\nabla p + \rho \vec{g} + \vec{F} + \nabla(\bar{\bar{\tau}}) \tag{3}$$

As the effect of gravity and external forces are not considered, thereby the terms $\rho \vec{g}$ and $\vec{F}$ are neglected. Therefore, the equations for axial momentum and radial momentum can be written as

$$\frac{\partial}{\partial t}(\rho v_x) + \frac{1}{r}\frac{\partial}{\partial x}(r\rho v_x v_x) + \frac{1}{r}\frac{\partial}{\partial r}(r\rho v_r v_x) = -\frac{\partial p}{\partial x} + F_x + \frac{1}{r}\frac{\partial}{\partial x}\left[r\mu\left(2\frac{\partial v_x}{\partial x} - \frac{2}{3}(\nabla.\vec{v})\right)\right] + \frac{1}{r}\frac{\partial}{\partial r}\left[r\mu\left(\frac{\partial v_x}{\partial r} + \frac{\partial v_r}{\partial x}\right)\right] \tag{4}$$

$$\frac{\partial}{\partial t}(\rho v_r) + \frac{1}{r}\frac{\partial}{\partial x}(r\rho v_x v_r) + \frac{1}{r}\frac{\partial}{\partial r}(r\rho v_r v_r) = -\frac{\partial p}{\partial r} + F_r + \frac{1}{r}\frac{\partial}{\partial r}\left[r\mu\left(2\frac{\partial v_r}{\partial r} - \frac{2}{3}(\nabla.\vec{v})\right)\right] + \frac{1}{r}\frac{\partial}{\partial x}\left[r\mu\left(\frac{\partial v_x}{\partial r} + \frac{\partial v_r}{\partial x}\right)\right] - 2\mu\frac{v_r}{r^2} + \frac{2}{3}(\nabla.\vec{v}) + \frac{2}{3}\frac{\mu}{r}(\nabla.\vec{v}) \tag{5}$$

The velocity field is

$$\nabla.\vec{v} = \frac{\partial v_x}{\partial x} + \frac{\partial v_r}{\partial r} + \frac{v_r}{r} \tag{6}$$

Since the simulation is performed at a constant temperature, the energy equation is no longer needed in the mentioned case. The above equations, when solved, will give the velocity field of the formed droplet of AuNPs ink.

In ANSYS fluent for multiphase flow, the equations applied for each Eulerian phase will individually give the velocity field of the phases. The continuity equation for the secondary phase (AuNPs ink) will be

$$\frac{1}{\rho_b}\left[\frac{\partial}{\partial t}(\psi_b \rho_b) + \nabla(\psi_b \rho_b \vec{v}_b)\right] = \frac{1}{\rho_b}\left[\sum_{a=1}^{n}(\dot{m}_{ab} - \dot{m}_{ba})\right] \tag{7}$$

where suffix a and b represent the properties of air and AuNPs ink, ρ is the density, ψ is the volume fraction, $\dot{m}_{ab}$ is the mass transfer from phase a to b, and $\dot{m}_{ba}$ is the mass transfer from phase b to a. For the primary phase, another constraint is used to compute the volume fraction of air, i.e., the sum of total volume fractions of phases in a cell equals 1. The simulation is formulated in explicit form, and therefore the momentum equation is

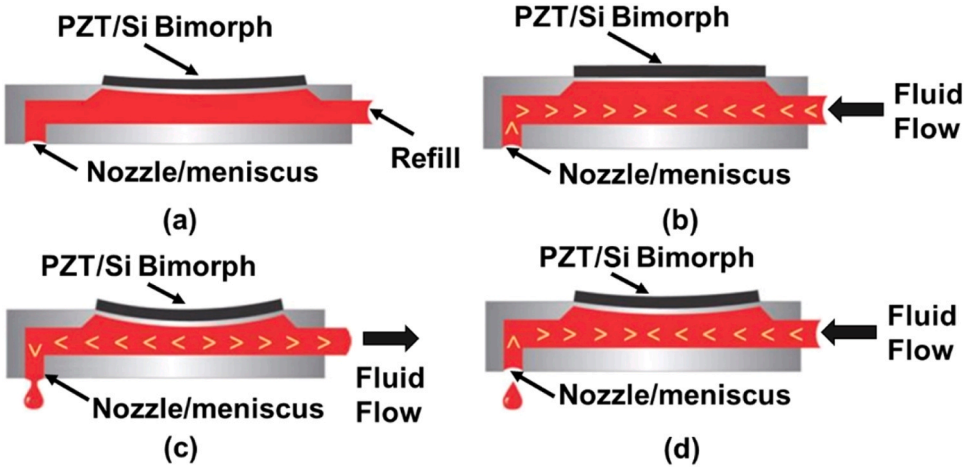

Fig. 1. Schematic illustration of the working of a piezoelectric-based DoD printing process.
Adapted with permission from Haque et al. [12], © 2016 AIP Publishing LLC.

$$\frac{\psi_b{}^{n+1}\rho_b{}^{n+1} - \psi_b{}^{n}\rho_b{}^{n}}{\Delta t} V + \sum_f \left(\rho_b U_f^n \psi_{b,f}^n\right) = \left[\sum_{a=1}^{n} (\dot{m}_{ab} - \dot{m}_{ba})\right] V \quad (8)$$

2.2.3. Domain modeling and meshing

The design of the nozzle and simulation domain is created using the Design Modeler subsystem of ANSYS Workbench. A triangle-based, size-refined discretization/meshing scheme generates the mesh. The average size of the triangle face is 5 * 10^{-6} m. The named selections for inlet, outlet, axis, hydrophilic wall (nozzle), and hydrophobic wall (nozzle) are created, as shown in Fig. 4.

2.2.4. Boundary conditions

A user-defined function (UDF) for the spatial and temporal velocity through the nozzle inlet is programmed using the C language mentioned in the Supporting Information (Section 1) *titled "User-defined Function for the Modeling of AuNPs ink Droplet Formation through DoD Regime"*. This defined function is hooked up to the model after getting processed through the interpreter. The volume fraction of ink at the inlet and the fraction of backflow through the pressure outlet are defined. The equations are solved with a first-order implicit transient formulation, and the duration of the simulation run is 120 microseconds with a time step size of 0.1 microseconds.

2.3. IJP of AuNPs ink

Identifying the appropriate substrate material is required before starting the IJP process using the formulated AuNPs ink. Among the different types of substrates available in the market, using inkjet-based photo papers has the advantage of being easy to use and dispose of, low cost, eco-friendly, recyclable, and bio-degradable. The success of using coated papers in pH and gas sensors was phenomenal and readily available in the market. Because of such success, there is growing interest in producing low-cost paper-based sensors. The wettability behaviour of photo papers is far better than non-porous substrates such as plastic films, glass, and silicon wafers. In this study, the Kodak professional inkjet photo paper (Specifications: Premium photo glossy paper, Size - A4 (210 *297 mm), Mass – 270 g/m2 with 5760 DPI, Manufacturer - Kodak, India). is used as the substrate material for the IJP deposition.

The inkjet printer used in the printing of AuNPs ink is the R&D benchtop deposition-based FUJIFILM Dimatix DMP-2831 utilizing a disposable piezoelectric inkjet cartridge as shown in Fig. 5**a).** The DMP-2831 allows the deposition of customized fluidic materials ranging from gels to inks on an 8 * 11 in. or A4 sized substrate. This micro-precision jetting of customized NP-based ink can create and define patterns over an area of about 200 * 300 mm^2 and handle substrates up to 25 mm thick with an adjustable Z height. The temperature of the vacuum platen in the printer, which places the substrate in place, can be adjusted to 60 °C. The DMP-2831 offers a variety of patterns using a pattern editor program on the substrate ranging from porous to non-porous. This system enables easy printing of structures and samples for process verification and prototype creation. The value of nozzle diameter (d_{nozzle}) of DMP 2831 printer is 21.5 μm [46]. The technical specifications for DMP 2831 are enlisted in *Section 2* ***in*** Supporting Information.

Table 2
Measured average density, ST, and viscosity with SD of AuNPs ink with varying Au concentration.

S. No.	[Au] of AuNPs ink (ppm)	Density (kg/m^3)	ST (mN/m)	Viscosity (cP)
1	300	1001	45.04 ± 0.15	2.5 ± 0.7
2	600	1048	51.60 ± 0.14	4.2 ± 0.24
3	1200	1132	55.00 ± 0.30	5.8 ± 0.29

The initial parameters used in the IJP of AuNPs ink for DMP-2831 printer are: Head Angle: 4.5°, Substrate Temperature: 30 °C, Substrate Thickness: 250 μm, Voltage: 10–20 V, increment in volt: 1.0 V, Temperature (cartridge): 30.0 °C, Jets in Use: 16 Nozzles, Cartridge Print Height: 1.000 mm, Substrate Pattern – X (width): 75.584 mm, Y (height): 101.00 mm, Drop Spacing 64 μm (397 DPI). The following procedure is used for filling the AuNPs ink in the cartridge reservoir. 1.5 ml of the formulated AuNPs ink was filled in the empty reservoir through the syringe. After filling it, the reservoir is closed with the nozzle head. The whole inkjet cartridge head with the reservoir is locked in the printer, and the rectangular pattern is selected. The rectangular-shaped pattern is printed on the paper substrate with 5, 10, and 25 repetitions in the IJP process.

The voltage waveform used in the IJP of AuNPs ink and the schematic diagram of the printhead of DMP 2831 for driving the piezoelectric crystal in the print head are shown in Fig. 5**b) and c),** respectively. It consists of two pulses (i) Primary and (ii) Secondary pulse. The waveform starts at $V_0 = 0$ V when t = 0 μs while the primary and secondary pulse starts at the starting time duration 't_{fall1}' and 'T_{sec}'. The primary pulse has a complete-time duration of ($t_{fall1} + t_{echo} + t_{rise} + t_{dwell1} + t_{fall2} + t_{dwell2} + t_{fall3}$). The secondary pulse has a time period of T_{sec}, respectively. The nature of the primary pulse is bipolar, which includes two trapezoids of negative and positive voltages. These

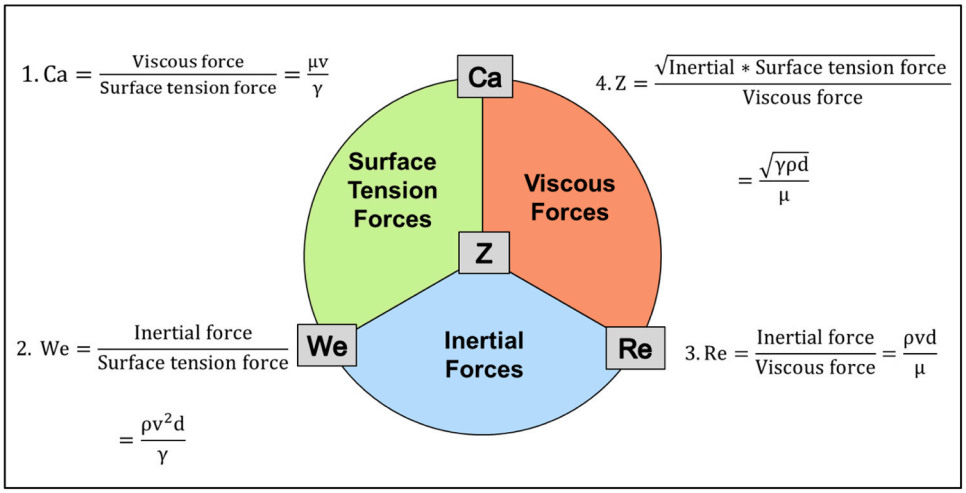

Fig. 2. Pie chart diagram for defining the following dimensionless numbers: Ca, We, Re and Z.

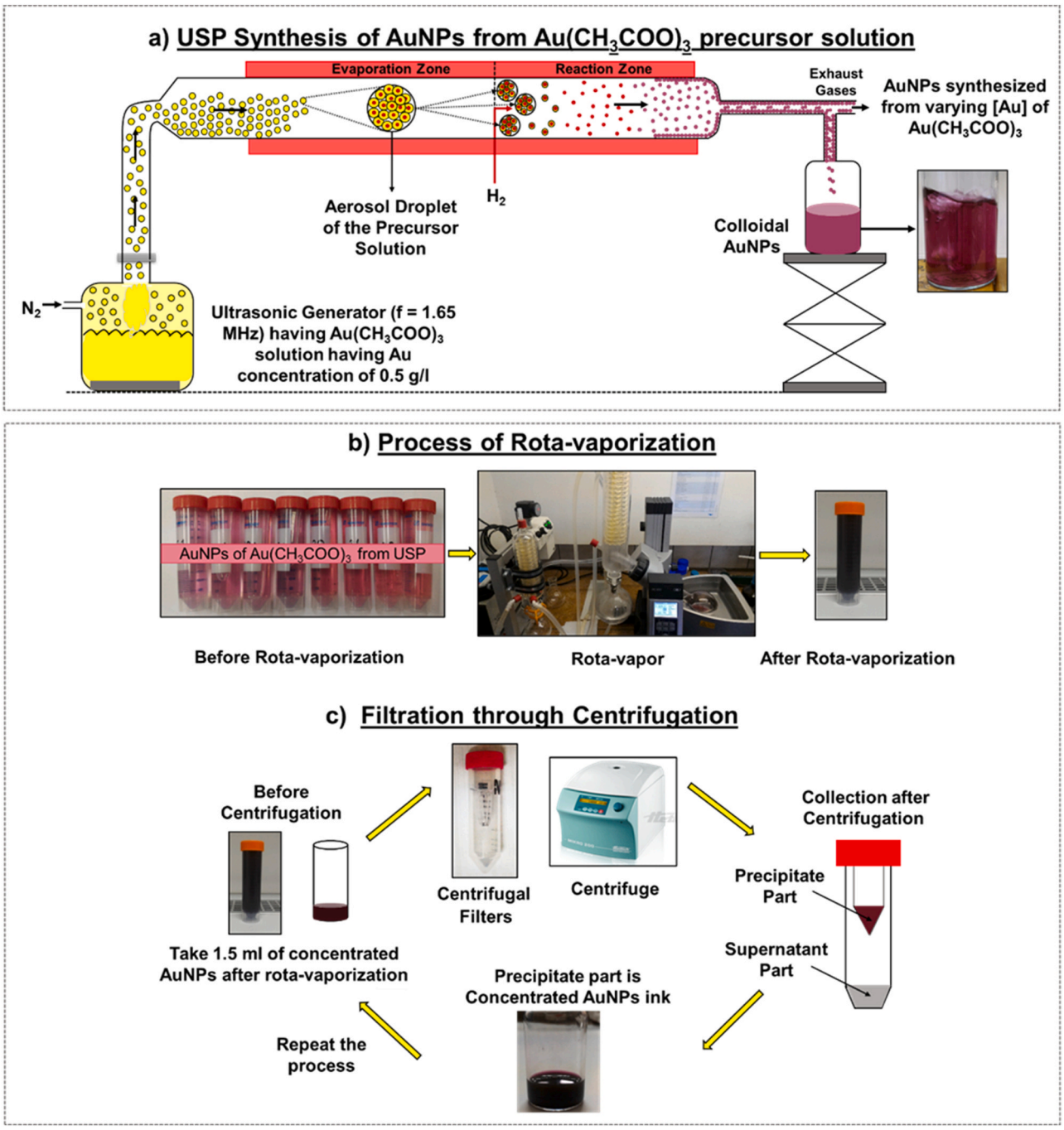

Fig. 3. represents **a)** USP synthesis of AuNPs by utilizing the 0.5 g/l concentrated of aqueous-based $Au(CH_3COO)_3$ precursor solution. AuNPs ink formulation via **b)** the process of rota-vaporization and **c)** filtration through centrifugation.

Table 3
USP synthesis parameters of AuNPs.

S. No.	Precursor	[Au] (g/l)	T_1 (°C)	T_2 (°C)	N_2 (l/min)	H_2 (l/min)
1	Gold (III) Acetate precursor solution $Au(CH_3COO)_3$	2–0.5	100	300	2–1	1–0.5

trapezoids have a minimum and maximum voltage of V_β and V_α, respectively. The primary pulse is designed to eject the AuNPs ink droplet of a predetermined volume through an activated inkjet-driven pulse voltage. The nature of the secondary pulse is unipolar and rectangular-shaped, having the maximum positive voltage of V_γ. The numeric value of the pulse voltage for the secondary pulse (V_γ) is always less than the primary pulse voltage (V_α). Each inkjet in the nozzle has a piezoelectric transducer that will be activated by these applied voltage waveforms. It causes the AuNPs ink meniscus in each inkjet to move from the nozzle.

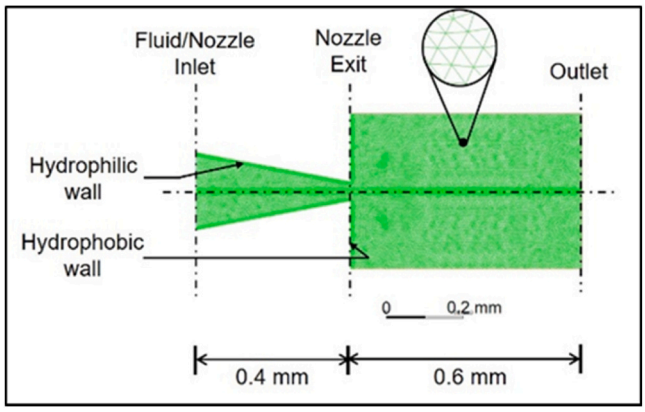

Fig. 4. shows the geometry of the nozzle and the mesh showing the named selections.

3. Results and discussion

3.1. Jettability window definition framework

The AuNPs synthesized from $Au(CH_3COO)_3$ precursor through USP were formulated into concentrated AuNPs ink using the process of rotavaporization, filtration, and centrifugation in three (3) concentration levels of 300, 600, and 1200 ppm. The yield efficiency of the AuNPs synthesized by USP process is an important consideration for the synthesis process. It can be calculated as the ratio of amount of the AuNPs produced to precursor of $Au(CH_3COO)_3$ used. The precursor concentration used is 0.5 g/l and its consumption in one run of experiment of 4 h is 0.4 L. The volume of the AuNPs synthesized with final concentration of 300 ppm is 0.5 L. Therefore, the yield efficiency of the USP process is calculated as 75% (*Calculations are available in the Section 3* ***in SI***).

The empirical relation for calculating the minimum velocity needed for ejecting the AuNPs ink droplet from the nozzle is mentioned in Eq. 9.

$$v_{(\min)\text{drop}} = \sqrt{\left(\frac{4X \quad Surface \quad Tension(N/m)}{Density(kg/cm^3)X \quad d_{nozzle}(m)}\right)} \tag{9}$$

After the ink droplet formation and ejection from the nozzle, a series of droplets will be ejected for the applied pressure pulse. This ejection of the series of droplets will form an initial fluid jet. The fluid jet velocity (v_{jet}) will always be greater than the drop ejection velocity because of the significant momentum [37]. To calculate the AuNPs inkjet velocity, the model derived by Driessen and Jeurissen [38] and Djiksman [39] is used. The volume of the AuNPs ink drop ejected (V_{drop}) is defined by integrating the ink flow rate through the nozzle of the cartridge (Eq. 10). Taking the circular section of the nozzle of the cartridge having the radius 'r_{nozzle}'.

$$V_d = \int_{t_1}^{t_2} \pi r_{nozzle}^2 v_{jet} dt \tag{10}$$

Here, t_1 = time interval during the AuNPs ink flows towards the nozzle to form the initial inkjet and t_2 = time interval when the flow reverses its direction. There will be a reduction in the momentum of the AuNPs ink in motion due to the following phenomena: viscous energy dissipation during the ink droplet formation and shrinkage in the neck as

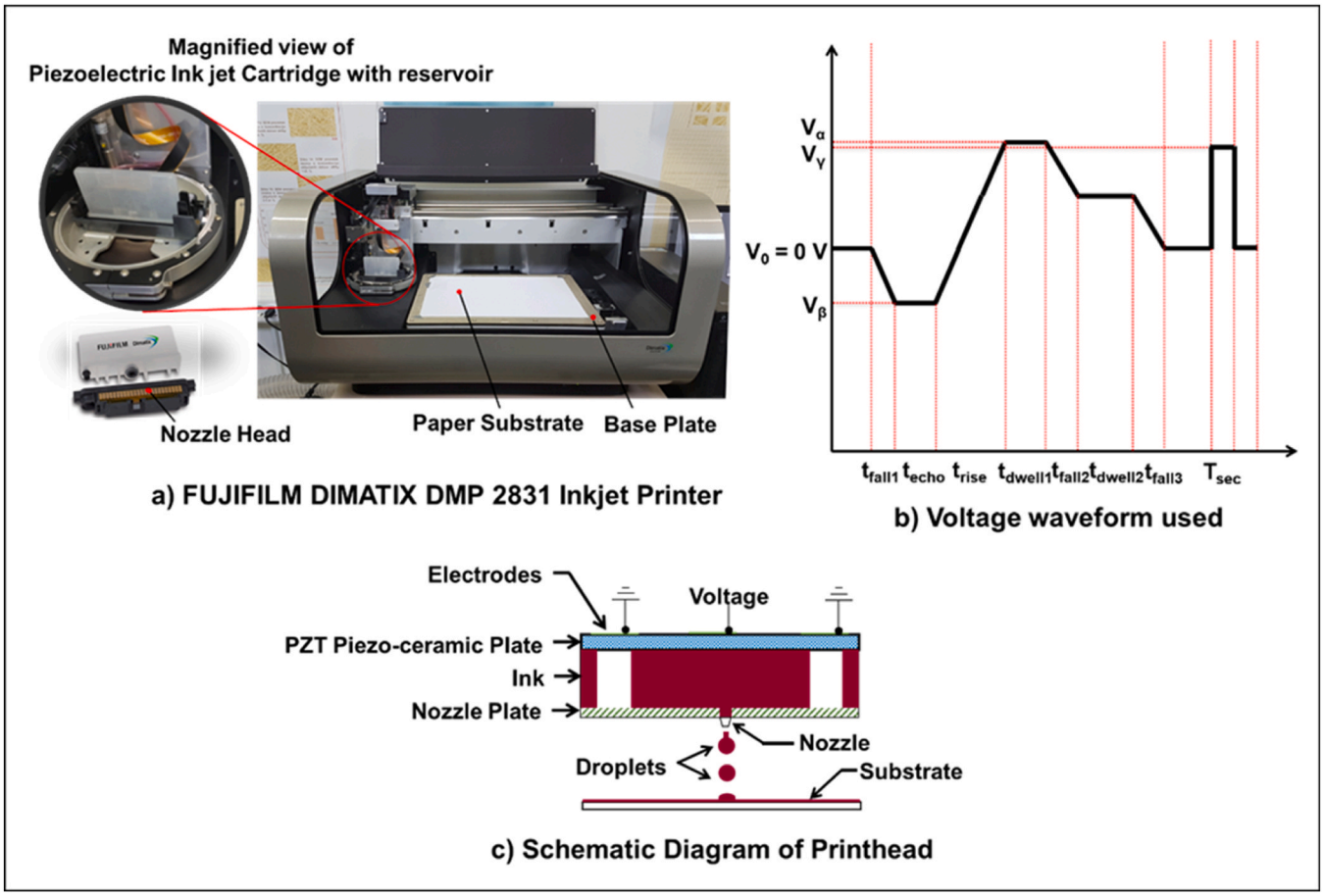

Fig. 5. shows **a)** FUJIFILM Dimatix DMP-2831 inkjet printer used for printing patterns using AuNPs ink of 1200 ppm synthesized from USP, **b)** a Voltage waveform used, and **c)** a Schematic diagram of the printhead.

it separates from the inkjet. This momentum transfer ($\dot{m}_n$) during these processes is given by Eq. 11.

$$\dot{m}_n = -3\pi r_{nozzle}^2 \mu \tag{11}$$

Here, μ is the viscosity of the AuNPs ink.

The capillary force will be the main contributing force that restricts the ink motion from the nozzle. Therefore, the resulting momentum change is given by

$$\dot{m}_c = -(t_1 - t_2)\pi r_{nozzle}\gamma \tag{12}$$

Here, γ is the ST of the AuNPs ink.

Thus, the expression for the ejected drop velocity incorporating the momentum change from all the sources will be

$$v_{drop} = \frac{1}{\rho V_d}\left[\int_{t_1}^{t_2} \rho\pi r_{nozzle}^2 v_{jet} dt - 3\mu\pi r_{nozzle}^2 - (t_2 - t_1)\pi r_{nozzle}\gamma\right] \tag{13}$$

Assuming the AuNPs ink flow to be modeled for the fixed period, constant velocity without viscous dissipation.

$$\delta t = (t_1 - t_2) \tag{14}$$

$$V_{drop} = \pi r_{nozzle}^2 v_{jet}\delta t \tag{15}$$

The equation becomes

$$v_{jet}^2 - v_{jet}v_{(\min)drop} - \frac{3\mu}{\rho\delta t} - \frac{\gamma}{\rho r_{nozzle}} = 0 \tag{16}$$

Here, the v_{jet} can be obtained for the minimum drop velocity. The optimum range of the values for δt can be taken between 3 μs and 7 μs [47]. In our case, it is taken as 7 μs. The $v_{(min)drop}$ and v_{jet} velocities were calculated for the AuNPs inks of varying concentrations of [Au] from the inkjet printer having the nozzle diameter (d_{nozzle}) of 21.5 μm (Table 4).

After theoretically calculating the minimum velocity needed for the drop formation and the final inkjet velocity of AuNPs ink, the jettability window defined by Ca, We and Z numbers are developed for the following range of velocities: $v_1 = 3$ m/s, 2. $v_2 = 3.5$ m/s, 3. $v_3 = 4$ m/s and 4. $v_4 = 4.5$ m/s for the varying concentrations of 300, 600 and 1200 ppm as shown in Table 5.

Each data point on the graphs in Fig. 6 represents a single AuNPs ink of a specific Au concentration at a specific mentioned velocity. Thereby, the lines represent the behaviour of the specific concentrated ink at multiple velocities ranging from the drop formation to the fluid jet velocity. These velocities can be controlled by changing the pulse voltage in the printer. The Ca and We jettability window **in** Fig. 6**a** has linear and quadratic ink drop velocity dependence. Therefore, the log–log plot will produce contour lines with a slope of ½ for each formulated AuNPs ink of varying concentrations. The Z of AuNPs ink of 300 ppm for the nozzle dia of 21.5 μm is 12.45. The Z value exceeds the upper limit of the printability range 10. A high value of Z results in the formation of multiple satellite drops. The viscosity is too low for the stable and single droplet formation and fluid jet for good printability. This behaviour of low viscous fluid is consistent with the reported works by Jang [41] and Reis & Derby [42].

As we look further into the increased concentration of the AuNPs ink from 300 ppm to 600 ppm, the viscosity increases from 0.0025 ± 0.0007–0.0042 ± 0.0024 Pa.s. The Z value is 8.11, falling in the printability range of $1 \leq Z \leq 10$. With the Au content of 600 ppm in ink, the droplets shall be a bit stable. However, it could not persist long enough to satisfy the jettability criterion. The viscosity of the AuNPs ink of 1200 ppm further increases to 0.0058 ± 0.0029 Pa. s, reducing the Z value to 6.30. This value of the viscosity is high enough that it results in the formation of a stable droplet and imparts good jettability. Although the AuNPs ink of 1200 and 600 ppm are jettable, with 600 ppm, its jettable condition lies near the maximum range of Z, i.e., near the boundary of the jettability window.

The low value of Z (less than 10) of highly concentrated AuNPs ink will result in a stable and single drop from the nozzle orifice. This printability indicates the region where viscous forces increase and play an essential role in droplet formation. While AuNPs ink with higher Z values (greater than 10) shall form liquid columns that readily pinch off. This ink will get leaked from the cartridge where the viscous forces lag and become low. The ink flow will form a liquid jet, causing splashing on the printing substrate.

In the reported literature by Liu and Derby [47] of the ink fluids with similar rheological properties, the range of printability for We number is $2 \leq We \leq 25$. When $We = 2$, it is the minimum value needed to overcome the minimum capillary forces for the ink droplet formation. While, at $We = 10$, the critical value above which the satellite formation of the AuNPs ink droplets will occur. In the case of AuNPs ink of 300 ppm, We number reached the value of 9.68 calculated at the velocity of 4.5 m/s, which is very near to the critical value as shown in Fig. 5.12. It may result in the satellite and multiple drop formation during printing. Thus, this satellite drop formation may destabilize the fluid flow and reduce printing quality. Thus, a larger volume of AuNPs ink will drop out from the orifice of the nozzle causing the leakage on the substrate. The We of

Table 4
presents the calculated values of minimum velocity needed for the droplet ejection and the jet velocity of AuNPs inks of varying concentrations of [Au] from the inkjet printer of nozzle diameter (d_{nozzle}) of 21.5 μm.

S. No.	[Au] of AuNPs ink (ppm)	d_{nozzle} (μm) = 21.5 μm	
		$v_{(min)drop}$ (m/s)	v_{jet} (m/s)
1.	300	2.89	4.49
2.	600	3.03	4.42
3.	1200	3.00	4.23

Table 5
represents the values of the dimensionless numbers (Re, Ca, We, and Z) of the AuNPs ink of 300, 600 and 1200 ppm for different velocities of 3, 3.5, 4 and 4.5 m/s and nozzle diameters of 21.5 μm.

AuNPs ink (ppm)	Velocity (m/s)	d_{nozzle} = 21.5 μm			
		Re No.	Ca No.	We No.	Z No.
300	1. $v_1 = 3.00$	25.83	0.17	4.30	12.45
	2. $v_2 = 3.50$	30.13	0.19	5.85	
	3. $v_3 = 4.00$	34.43	0.22	7.64	
	4. $v_4 = 4.50$	38.74	0.25	9.68	
600	1. $v_1 = 3.00$	16.09	0.24	3.93	8.11
	2. $v_2 = 3.50$	18.78	0.29	5.35	
	3. $v_3 = 4.00$	21.46	0.33	6.99	
	4. $v_4 = 4.50$	24.14	0.37	8.84	
1200	1. $v_1 = 3.00$	12.59	0.32	3.98	6.30
	2. $v_2 = 3.50$	14.69	0.37	5.42	
	3. $v_3 = 4.00$	16.78	0.42	7.08	
	4. $v_4 = 4.50$	18.88	0.48	8.96	

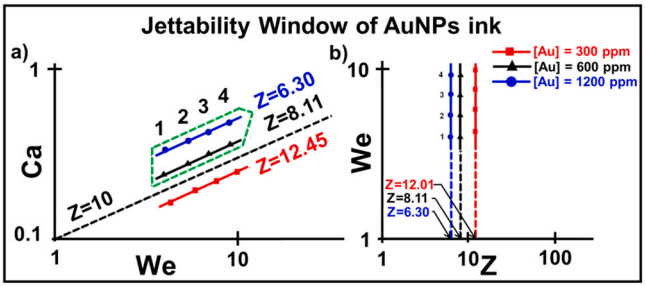

Fig. 6. shows **(a)** Ca-We and **(b)** We-Z jettability window of the formulated AuNPs ink of 300 (red line), 600 (black line) and 1200 ppm (blue line) determined at different velocities (1. 3 m/s, 2. 3.5 m/s, 3. 4 m/s and 4. 4.5 m/s) for the nozzle diameter (d_{nozzle}) of 21.50 μm.

AuNPs ink of 600 and 1200 ppm ranges from 3.66 to 8.96, which falls in the safe zone for stable drop formation, as represented in Fig. 6**b.**

As discussed above, for the jettability window framework for the AuNPs inks of varying concentration, ink of 1200 ppm had shown the most favourable properties that will be best suited for testing the ink through IJP for determining the printability characteristics.

3.2. IJP of AuNPs ink

The formulated AuNPs ink of 1200 ppm has shown the most favourable flow, rheological and jettable behaviour. The next framework measures the printability characteristics on the photo paper substrate, such as the morphology and the density of the printed AuNPs achieved through the *DMP 2831* printer. Before using this ink for printing, the theoretical simulation study is done to observe the ink droplet formation behaviour at different ink droplet velocities through a DoD inkjet printer using ANSYS Fluent software. The morphology of AuNPs in the printed patterns are characterized by the SEM technique for various repetitions in the printing process.The process parameter, such as pulse actuation voltage, is controlled and optimized to improve printing characteristics.

Before the printing process, the physical characterization of the AuNPs ink of 1200 ppm is carried out with the help of the following techniques: HRTEM-EDS, SEM-EDS, DLS and FTIR techniques. The morphology of the AuNPs in the concentrated ink is shown in Fig. 7**(a-b).** Mostly, the shape of these AuNPs can be depicted as ellipsoidal, while some are also spherical. The ellipsoidal AuNPs are multi-twinned and poly-dispersed, as shown in Fig. 7**(a-c).** The poly-dispersity nature of these AuNPs is due to coalescence and coagulation. This coalescence occurs due to the increased degree of mobility caused by the centrifugal forces applied during the purification and concentration process of the AuNPs from USP into inks. The index planes of these AuNPs in the ink are identified in the diffraction pattern (Fig. 7**d)** marked in yellow colour. It describes the Fm-3 m space group corresponding to the FCC lattice structure. A spacing of 2.3 Å in Fig. 6**(c-d)** of the coalesced AuNPs from the concentrated ink is visible, corresponding to the (1, 1, 1) of the

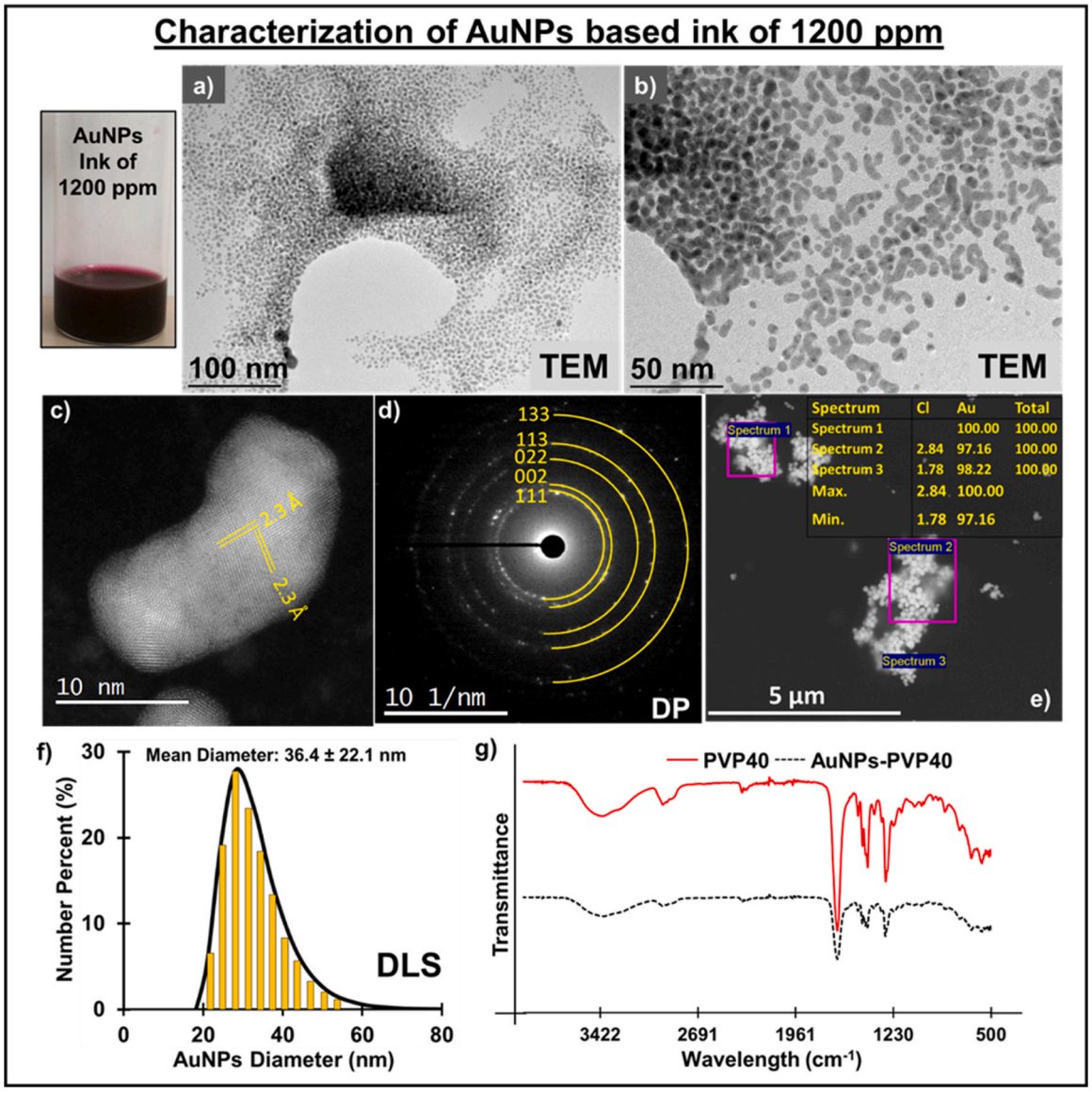

Fig. 7. (a, b) TEM characterization of the AuNPs ink of 1200 ppm, **(c)** TEM image of the single AuNP showing the spacing of 2.3 Å corresponding to the (1, 1, 1) Au plane, **(d)** ED pattern of AuNPs displaying several spots matching the lattice distances of Au and indicating the polycrystalline nature, **e)** EDX spectra showing the elemental composition, **f)** DLS size distribution of the AuNPs present in the ink**, g)** FTIR spectra of synthesized PVP40 stabilized AuNPs (black dotted curve) and pure PVP40 (red solid line curve) synthesized from the precursor of $Au(CH_3COO)_3$ through USP.

Au plane. The EDX spectrum of the AuNPs in the ink (Fig. 7**e)** detects the elemental composition as Au – (97.7 ± 1.1) wt% and Cl – (2.31 ± 0.53) wt%. With the help of DLS measurement **(**Fig. 7**f),** the peak size distribution of the AuNPs obtained through USP is 28% of the nanoparticles were present in the size range of 28.21 ± 5.2 nm while the average size distribution is 36.4 ± 22.1 nm. FTIR analysis confirms the PVP40-capping on the surface of AuNPs, as shown in Fig. 7**g.** The PVP40 spectrum shows its presence in C═O (1660 cm^{-1}) and C–N (1290 cm^{-1}). The FTIR spectrum of PVP40-coated AuNPs is similar to that of the original PVP40, although the differences were observed in the slight shift of wavenumber that confirms the PVP40 capping of AuNPs. The spectra of AuNPs from $Au(CH_3COO)_3$ are in good agreement with that reported by Dhumale et al. [48].

3.2.1. *Modeling of AuNPs ink droplet formation through DoD regime*

In the analysis, a single nozzle is modelled to eject the droplets of the ink into the stationary air at standard ambient conditions. This model comprises symmetrical features; therefore, only one side of the symmetrical geometry is modelled. The movement of the piezoelectric element above the nozzle causes the ejection of the ink droplet in the x-direction. The volume of fluid method is used for two immiscible fluid phases. The considered primary and secondary phases are air and AuNPs ink, respectively. The calculated Re number value lies well in the laminar flow range; thus, turbulence is not considered. As it is very challenging to emulate the action of the piezo element, time-dependent inlet velocity is defined. The simulations are run at two different ink droplet velocities of 3 and 4.5 m/s, as shown in Fig. 8**.** The values of the AuNPs ink properties are taken according to Table 2**.** The lower and higher velocity values of 3 and 4.5 m/s are taken based on the calculations for the minimum velocity needed for the ejection of the ink droplet ($v_{(min)drop}$) for 1200 ppm, as mentioned in Table 4**.**

When the AuNPs ink droplet velocity is 3 m/s, a single and stable droplet is formed at 40 μs. While at a higher velocity of 4.5 m/s, the ink droplet is formed with a long tail at just 20 μs (i.e., half of the above case). Due to this long tail formation, the ink droplet is fragmented into smaller fractions, leading to the multiple droplet formation. It could become a constraint for achieving a high resolution and accuracy in the printing process at a higher velocity. The lower velocity of 3 m/s will result in the precise deposition of the AuNPs ink of 1200 ppm with such a range of diameter nozzle printer. Therefore, the simulated single and stable droplet formation behaviour needs to be achieved by optimizing the design of the actuation pulse of the printhead of the inkjet printers. The actuation pulse voltage can be varied to control the velocity and ejected volume of the formulated ink droplet during the IJP process, as per agreement with [49].

3.2.2. *IJP of AuNPs ink of 1200 ppm using different DoD technology*

The DMP-2831 printer uses the FUJIFILM Dimatix's proprietary Silicon MEMS technology-based DMC-11610 cartridge having 16 nozzle jets. Before starting the printing process, the drop generator is actuated using a specific waveform having a peak voltage ranging from 10 to 40 V. The secondary waveform of the small amplitude is programmed, which cannot be avoided while printing the patterns using AuNPs ink. Initially, the pulse voltage (V_α) is set to a value of 15 V. With this value of actuation voltage, there is no ejection of droplets, and thus, no deposition of AuNPs ink is observed on the photo paper substrate. The pulse

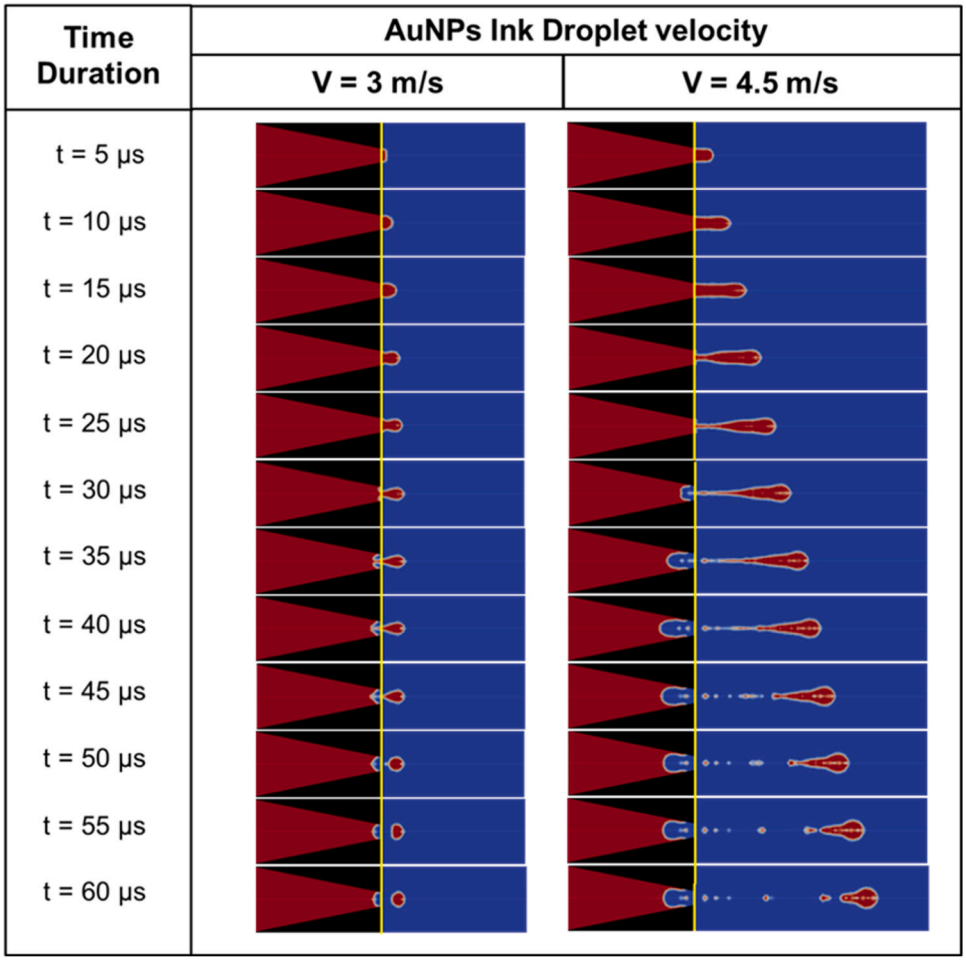

Fig. 8. Simulation of AuNPs ink droplet formation at droplet velocity of 3 m/s and 4.5 m/s respectively.

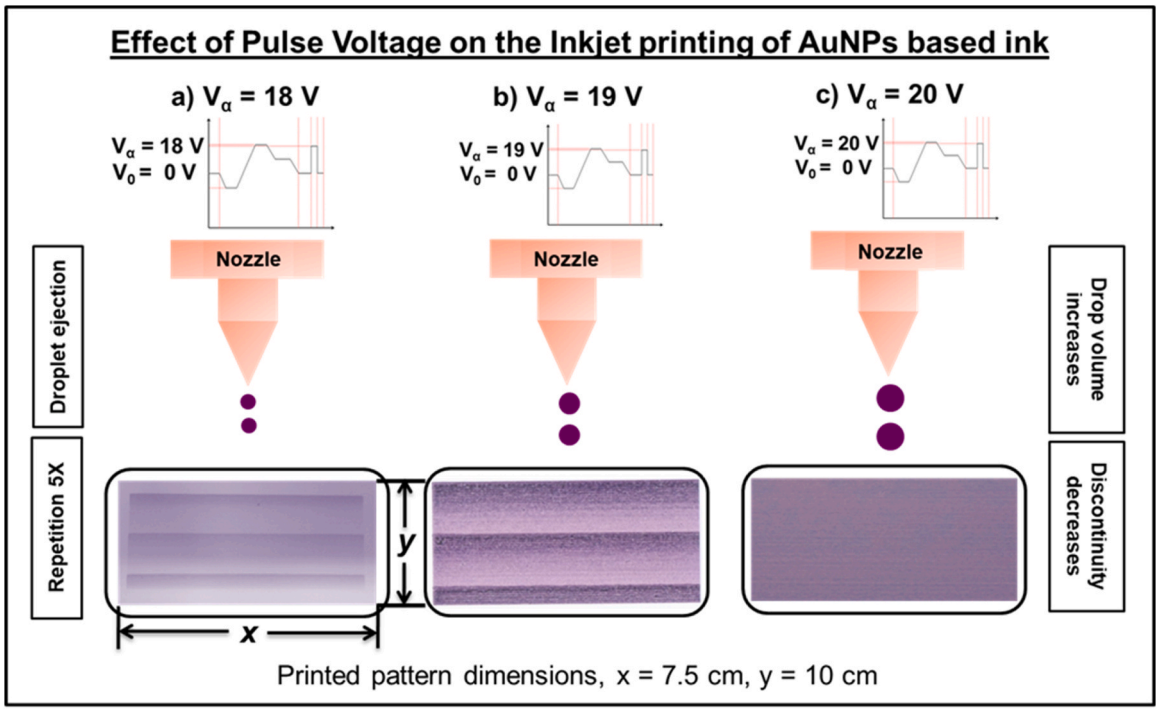

Fig. 9. represents the effect of the pulse voltage (V_α) of the nozzle on the IJP of AuNPs ink using DMP 2831 printer at **a)** 18 V, **b)** 19 V and c) 20 V.

voltage is increased by 1 V in each step, raising it to 17 V. With the pulse voltage of 17 V, similar observations are made, resulting in the unsuccessful printing of the AuNPs ink. As the pulse voltage is further increased to 18 V, the drop ejection from the nozzle head starts, and the printing is evident on the photo paper substrate in Fig. 9**a).** During the printing of the rectangular planar pattern, the printer prints in three cycles. At the start of each cycle, the first few lines are visible on the paper and disappear, leaving it blank. Therefore, it can be observed that the 18 V is not enough to have continuous droplet formation and printing of the selected rectangular pattern.

The pulse voltage is increased to 19 V to see its influence on the continuity of the pattern. Fig. 9**b)** shows more deposition of the AuNPs ink on the paper substrate by increasing the pulse voltage to 19 V. It can be depicted that the volume of the ejected drop increases as compared to the volume dispensed by the lower values. In this case, the unprinted portion is decreased.

Finally, the pulse voltage is increased to the maximum value of 20 V. The continuous deposition of AuNPs ink achieved on the paper substrate, as shown in Fig. 9**c).** There are no discontinuities present on the pattern. This voltage value indicates the maximum volume of droplets achieved to print the continuous rectangular pattern. Therefore, the minimum voltage needed to eject the AuNPs ink droplet is 18 V; below this voltage, there is no AuNPs droplet formation and nozzle ejection, while the optimum voltage required to discharge the maximum volume of the droplet is 20 V. The following observation can be concluded that a higher pulse voltage of 20 V was required to continuously eject the concentrated AuNPs ink. With higher pulse voltage, the piezoelectric element in the nozzle will result in more contraction and expansion,

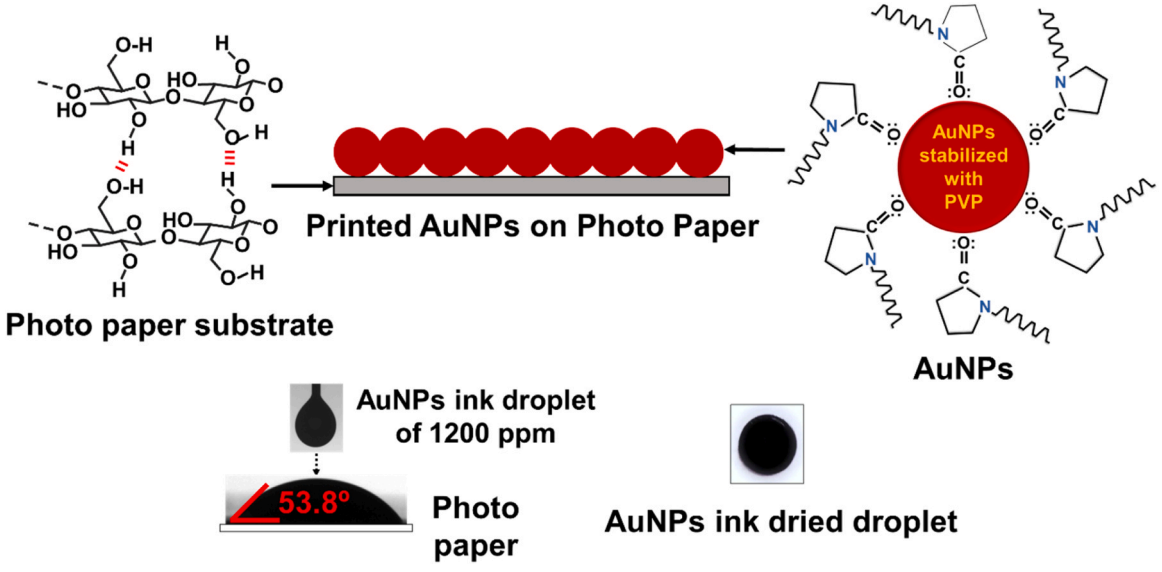

Fig. 10. Surface chemistry and interaction of AuNPs ink on inkjet-based photo paper.

resulting in the large-sized and continuous droplet formation and ejection for these types of AuNPs ink.

The surface chemistry and interaction of AuNPs ink on inkjet-based photo paper are complex and involve wetting, absorption and adhesion processes **(**Fig. 10**).** The photopaper used in the study have the characteristic pore size in the range of 40–400 nm which is small enough to allow the printed film of AuNPs with an average diameter of approximately 50 nm. The paper has a weak negative charge due to the presence of the hydroxyl groups of cellulose [50]. The AuNPs are well adsorbed on the paper substrate even though, both the materials were negatively charged. The high adsorption of AuNPs on the cellulose fibres as evident in Fig. were achieved by the van der Waals binding without any retention aid. The attachment of the AuNPs on paper is controlled by the 3D network of paper, which consists of a large volume fraction of pores providing strong capillary forces for the diffusion of AuNPs from solution[51]. The contact angle represents surface tension and surface energy difference between the AuNPs ink droplet and photo paper substrate. It is measured as 53.8º signifying the hydrophilic behavior of the ink. The wetting behaviour has shown a good combination of ink spreading and penetration providing a good ink setting **(**Fig. 10**)** It is due to the presence of lower water content that resulted in the uniform drying of the ink droplet.

The morphology of the NPs in the ink formulation affects the droplet impact behavior and droplet velocity in IJP process. In case of spherical and nanoplatelets shaped particles, the ink droplet velocity increases with an increase in pulse driving voltage. In the printing of nanoplatelets composed ink, it is difficult to control the ejection of the droplets because of the formation of satellite droplets as the change in the drop direction starting from the first printings. In case of spherical particles, satellite droplet formation occurs but reabsorbed with the main drop during jetting as evident in the simulation also **(**Fig. 8**)** [52,53].

Particle size dominates the droplet behavior in respect to the contact angle and diameter. As the particle size increases, the wetting diameter also increases. It indicates that the printing of large particle will result in

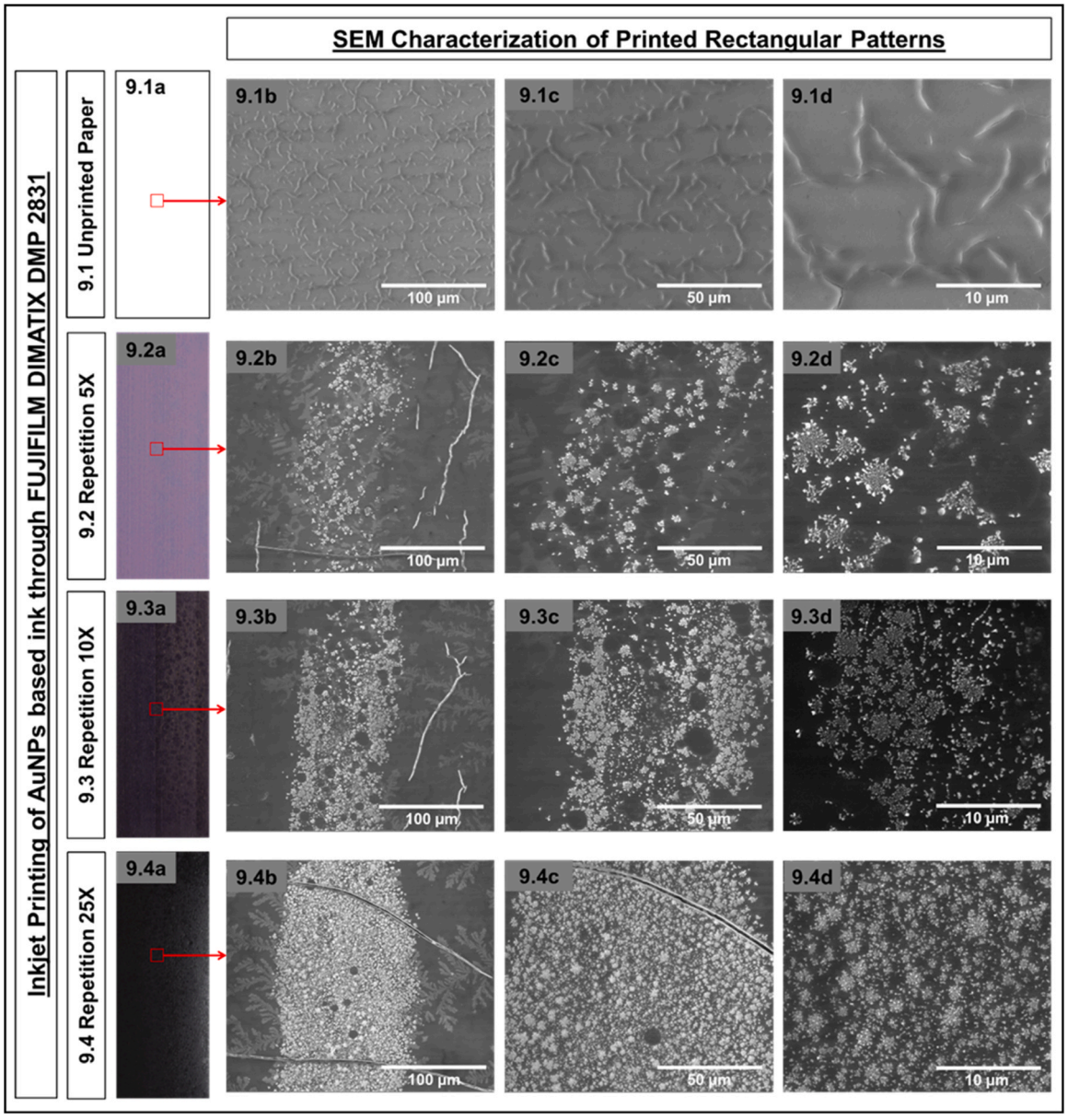

Fig. 11. represents the unprinted and printed rectangular patterns on photo paper obtained through the IJP of AuNPs ink using DMP 2831 printer with different repetitions and its SEM characterization. **9.1(a)** and **9.1(b-d)** showed the image and its SEM characterization of the unprinted photo paper substrate respectively. **9.2 (a), 9.3(a), 9.4(a)** showed the images and **9.2(b-d), 9.3(b-d), 9.4(b-d)** its SEM characterization of the printed photo paper with 5 × , 10 × and 25 × repetitions respectively.

the larger dot or wider line width. While the small particles possess extra mobility to flow tending for coffee ring effects and vice versa. Large particle tends to settle down with coffee ring effects. Ink with smaller sized particles have greater number of particles dispersed in the droplet that provides larger total surface area compare to large sized particle formulated ink. The total charge on the smaller particles would be greater than the charge on larger particles. This excess charge provide an increase in surface energy, therefore the larger contact angle. It also influences the initial velocity of the ink droplet. The large charge provides the large electronic force that has the high electric field acceleration force. It results in the high impact velocity of ink droplet that can cause splashing of the droplet impacting the resolution of the print [54,55].

Fig. 11 shows the unprinted and printed rectangular patterns using the DMP 2831 printer of 5 ×, 10 ×, and 25 ×, respectively. The morphological characterization is performed on these printed patterns by SEM to visualize the density of AuNPs distribution after printing in different magnification scales. Firstly, the unprinted paper is characterized, and the cracks that appeared on the unprinted paper can be identified in Fig. 11**.1(a-d).** The AuNPs ink is printed for 5 × repetitions on the substrate, as shown in Fig. 11**.2(a),** followed by the characterization in Fig. 11**.2(b-d)**. The density of the AuNPs distribution is low as the clusters of these particles are significantly apart. The AuNPs are absorbed by the fibres and the cracks, which are present in low quantity.

In the printed pattern of AuNPs ink on the paper substrate with 10 × repetitions in Fig. 11**.3(a-d),** the density of AuNPs clusters increases, and the particles are placed nearer. The discontinuities are observed in the patterns between the clusters of AuNPs on the substrate surface. The AuNPs printed patterns of 25 × repetition on paper substrate are present in high density without discontinuities, as shown in Fig. 11**.4(a-d).** The clusters of AuNPs were placed near each other without any presence of discontinuities. Among the 5 ×, 10 ×, and 25 × repetitions with DMP-2831 printer, the maximum repetitions of 25 × repetitions resulted in continuous distribution of the AuNPs clusters on paper substrate.

4. Conclusions

This research provides the jettability window definition framework of Ca-We and We-Z calculated for different velocities of AuNPs inks starting from the droplet formation (3 m/s) to the fluid jet (4.5 m/s). The most important findings are the following:

The formulated AuNPs ink with a concentration of 1200 ppm belongs to the printability range $1 < Z < 10$ and enables the formation of stable droplets and imparts good jettability at lower droplet velocity (3 m/s). On the contrary, higher velocity (4.5 m/s) caused the multiple drop formation, making AuNPs ink jet unstable.

The AuNPs ink of 1200 ppm has shown the most favourable properties, as confirmed by the IJP use of Dimatix DMP-2831 printer with various repetitions performed on the paper substrate. It was experimentally confirmed that high uniformity and continuity of AuNPs were achieved by varying the pulse activation voltage from 18 V to 20 V.

AuNPs inks with concentrations of 600 and 300 ppm had unstable jettable behaviour, which may result in splashing.

CRediT authorship contribution statement

MS, RR, SC, RK, and ARD conceived and designed the work. MS, RR, PM, RK, BF, ANG and ARD performed the experiments, characterization, simulation and analysis. Finally, MS, RR, SC, and ARD, wrote the manuscript.

Declaration of Competing Interest

The authors declare that they have no known competing financial interests or personal relationships that could have appeared to influence the work reported in this paper.

Data Availability

Data will be made available on request.

Acknowledgement

The author(s) acknowledge the Erasmus Mundus, Lot 13 Euphrates Program Project Number – 2013-2540/001-001-EMA2 for providing the doctoral mobility research fellowship.

Appendix A. Supporting information

Supplementary data associated with this article can be found in the online version at doi:10.1016/j.colsurfa.2023.132837.

References

[1] C. Waldner, A. Ritzer, U. Hirn, Modeling inkjet dots from drop spreading, absorption and evaporation – An engineering approach, Colloids Surf. A Physicochem Eng. Asp. 674 (2023), 131986, https://doi.org/10.1016/j.colsurfa.2023.131986.

[2] L. Nie, Y. Chen, Y. Dong, R. Li, G. Chang, Development of high-performance, chemical pretreatment-free dye-based inks for digital printing on polyester fabric, Colloids Surf. A Physicochem Eng. Asp. 678 (2023), 132470, https://doi.org/10.1016/j.colsurfa.2023.132470.

[3] C. Gao, Y. Zhang, S. Mia, T. Xing, G. Chen, Development of inkjet printing ink based on component solubility parameters and its properties, Colloids Surf. A Physicochem Eng. Asp. 609 (2021), 125676, https://doi.org/10.1016/j.colsurfa.2020.125676.

[4] A. Fraters, R. Jeurissen, M. van den Berg, H. Reinten, H. Wijshoff, D. Lohse, M. Versluis, T. Segers, Secondary tail formation and breakup in piezoacoustic inkjet printing: femtoliter droplets captured in flight, Phys. Rev. Appl. 13 (2020) 24075, https://doi.org/10.1103/PhysRevApplied.13.024075.

[5] J. Li, F. Rossignol, J. Macdonald, Inkjet printing for biosensor fabrication: combining chemistry and technology for advanced manufacturing, Lab Chip 15 (2015) 2538–2558, https://doi.org/10.1039/C5LC00235D.

[6] G. Kollamaram, S.C. Hopkins, B.A. Glowacki, D.M. Croker, G.M. Walker, Inkjet printing of paracetamol and indomethacin using electromagnetic technology: rheological compatibility and polymorphic selectivity, Eur. J. Pharm. Sci. 115 (2018) 248–257, https://doi.org/10.1016/j.ejps.2018.01.036.

[7] E. Tekin, P.J. Smith, U.S. Schubert, Inkjet printing as a deposition and patterning tool for polymers and inorganic particles, Soft Matter 4 (2008) 703–713, https://doi.org/10.1039/B711984D.

[8] K. Li, J. Liu, W. Chen, L. Zhang, Controllable printing droplets on demand by piezoelectric inkjet: applications and methods, Microsyst. Technol. 24 (2018) 879–889, https://doi.org/10.1007/s00542-017-3661-9.

[9] K. Li, J. Liu, W. Chen, L. Zhang, Controllable printing droplets on demand by piezoelectric inkjet: applications and methods, Microsyst. Technol. 24 (2018) 879–889, https://doi.org/10.1007/s00542-017-3661-9.

[10] L. Liu, Z. Shen, X. Zhang, H. Ma, Highly conductive graphene/carbon black screen printing inks for flexible electronics, J. Colloid Interface Sci. 582 (2021) 12–21, https://doi.org/10.1016/j.jcis.2020.07.106.

[11] J. Natsuki, T. Abe, Synthesis of pure colloidal silver nanoparticles with high electroconductivity for printed electronic circuits: The effect of amines on their formation in aqueous media, J. Colloid Interface Sci. 359 (2011) 19–23, https://doi.org/https://doi-org.egateway.vit.ac.in/10.1016/j.jcis.2011.03.079.

[12] R.I. Haque, R. Vié, M. Germainy, L. Valbin, P. Benaben, X. Boddaert, Inkjet printing of high molecular weight PVDF-TrFE for flexible electronics, Flex. Print. Electron. 1 (2016), 015001, https://doi.org/10.1088/2058-8585/1/1/015001.

[13] R. Taheri-Ledari, W. Zhang, M. Radmanesh, N. Cathcart, A. Maleki, V. Kitaev, Plasmonic photothermal release of docetaxel by gold nanoparticles incorporated onto halloysite nanotubes with conjugated 2D8-E3 antibodies for selective cancer therapy, J. Nanobiotechnol. 19 (2021), 239, https://doi.org/10.1186/s12951-021-00982-6.

[14] R. Taheri-Ledari, M.R. Ahghari, F. Ansari, M. Forouzandeh-Malati, S. S. Mirmohammadi, S. Zarei-Shokat, S. Ramezanpour, W. Zhang, Y. Tian, A. Maleki, Synergies in antimicrobial treatment by a levofloxacin-loaded halloysite and gold nanoparticles with a conjugation to a cell-penetrating peptide, Nanoscale Adv. 4 (2022) 4418–4433, https://doi.org/10.1039/D2NA00431C.

[15] R. Taheri-Ledari, A. Fazeli, A. Kashtiaray, S. Salek Soltani, A. Maleki, W. Zhang, Cefixime-containing silica nanoseeds coated by a hybrid PVA-gold network with a cys–arg dipeptide conjugation: enhanced antimicrobial and drug release properties, Langmuir 38 (2022) 132–146, https://doi.org/10.1021/acs.langmuir.1c02233.

[16] M. Segev-Bar, H. Haick, Flexible sensors based on nanoparticles, ACS Nano 7 (2013) 8366–8378, https://doi.org/10.1021/nn402728g.

[17] N. Komuro, S. Takaki, K. Suzuki, D. Citterio, Inkjet printed (bio)chemical sensing devices, Anal. Bioanal. Chem. 405 (2013) 5785–5805, https://doi.org/10.1007/s00216-013-7013-z.

[18] E.P. Hoppmann, W.W. Yu, I.M. White, Highly sensitive and flexible inkjet printed SERS sensors on paper, Methods 63 (2013) 219–224, https://doi.org/10.1016/j.ymeth.2013.07.010.
[19] M. Forouzandeh-Malati, F. Ganjali, E. Zamiri, S. Zarei-Shokat, F. Jalali, M. Padervand, R. Taheri-Ledari, A. Maleki, Efficient photodegradation of eriochrome black-T by a trimetallic magnetic self-synthesized nanophotocatalyst based on Zn/Au/Fe-embedded poly(vinyl alcohol), Langmuir 38 (2022) 13728–13743, https://doi.org/10.1021/acs.langmuir.2c01822.
[20] G. Sener, L. Uzun, A. Denizli, Colorimetric sensor array based on gold nanoparticles and amino acids for identification of toxic metal ions in water, ACS Appl. Mater. Interfaces 6 (2014) 18395–18400, https://doi.org/10.1021/am5071283.
[21] C.E. Krause, B.A. Otieno, A. Latus, R.C. Faria, V. Patel, J.S. Gutkind, J.F. Rusling, Rapid microfluidic immunoassays of cancer biomarker proteins using disposable inkjet-printed gold nanoparticle arrays, ChemistryOpen 2 (2013) 141–145, https://doi.org/10.1002/open.201300018.
[22] P. Ihalainen, F. Pettersson, M. Pesonen, T. Viitala, A. Määttänen, R. Österbacka, J. Peltonen, An impedimetric study of DNA hybridization on paper-supported inkjet-printed gold electrodes, Nanotechnology 25 (2014) 94009, https://doi.org/10.1088/0957-4484/25/9/094009.
[23] M. Rycenga, P.H.C. Camargo, Y. Xia, Template-assisted self-assembly: a versatile approach to complex micro- and nanostructures, Soft Matter 5 (2009) 1129–1136, https://doi.org/10.1039/B811021B.
[24] C. Hamon, S. Novikov, L. Scarabelli, L. Basabe-Desmonts, L.M. Liz-Marzán, Hierarchical self-assembly of gold nanoparticles into patterned plasmonic nanostructures, ACS Nano 8 (2014) 10694–10703, https://doi.org/10.1021/nn504407z.
[25] C. Hanske, E.H. Hill, D. Vila-Liarte, G. González-Rubio, C. Matricardi, A. Mihi, L. M. Liz-Marzán, Solvent-assisted self-assembly of gold nanorods into hierarchically organized plasmonic mesostructures, ACS Appl. Mater. Interfaces 11 (2019) 11763–11771, https://doi.org/10.1021/acsami.9b00334.
[26] A. Bastola, Y. He, J. Im, G. Rivers, F. Wang, R. Worsley, J.S. Austin, O. Nelson-Dummett, R.D. Wildman, R. Hague, C.J. Tuck, L. Turyanska, Formulation of functional materials for inkjet printing: a pathway towards fully 3D printed electronics, Mater. Today Electron. 6 (2023), 100058, https://doi.org/10.1016/j.mtelec.2023.100058.
[27] S. Conti, G. Calabrese, K. Parvez, L. Pimpolari, F. Pieri, G. Iannaccone, C. Casiraghi, G. Fiori, Printed transistors made of 2D material-based inks, Nat. Rev. Mater. 8 (2023) 651–667, https://doi.org/10.1038/s41578-023-00585-7.
[28] J. Li, E.H. Hill, L. Lin, Y. Zheng, Optical nanoprinting of colloidal particles and functional structures, ACS Nano 13 (2019) 3783–3795, https://doi.org/10.1021/acsnano.9b01034.
[29] E.H. Hill, C. Goldmann, C. Hamon, M. Herber, Laser-driven bubble printing of plasmonic nanoparticle assemblies onto nonplasmonic substrates, J. Phys. Chem. C 126 (2022) 7622–7629, https://doi.org/10.1021/acs.jpcc.2c02414.
[30] D. Yu, Y.-M. Shen, Y. Shen, W. Zhu, F.-Y. Han, A.-G. Shen, Visible security ink blended by Prussian blue analogues encapsulated gold (Au@PBA) nanoparticles for information hiding, Colloids Surf. A Physicochem Eng. Asp. 669 (2023), 131454, https://doi.org/10.1016/j.colsurfa.2023.131454.
[31] E. Maiorano, S. Gianvittorio, M. Lanzi, D. Tonelli, H. Pick, A. Lesch, Print-light-synthesis of gold thin film electrodes for electrochemical sensing, Adv. Mater. Technol. 8 (2023), 2202039, https://doi.org/10.1002/admt.202202039.
[32] E. Skotadis, J. Tang, V. Tsouti, D. Tsoukalas, Chemiresistive sensor fabricated by the sequential ink-jet printing deposition of a gold nanoparticle and polymer layer, Microelectron. Eng. 87 (2010) 2258–2263, https://doi.org/10.1016/j.mee.2010.03.001.
[33] V. Gubala, L.F. Harris, A.J. Ricco, M.X. Tan, D.E. Williams, Point of Care Diagnostics: Status and Future, Anal. Chem. 84 (2012) 487–515, https://doi.org/10.1021/ac2030199.
[34] A.L.M. Marsico, B. Creran, B. Duncan, S.G. Elci, Y. Jiang, T.B. Onasch, J. Wormhoudt, V.M. Rotello, R.W. Vachet, Inkjet-printed gold nanoparticle surfaces for the detection of low molecular weight biomolecules by laser desorption/ionization mass spectrometry, J. Am. Soc. Mass Spectrom. 26 (2015) 1931–1937, https://doi.org/10.1021/jasms.8b04922.
[35] G.B. Tezel, K. Arole, D.E. Holta, M. Radovic, M.J. Green, Interparticle interactions and rheological signatures of Ti3C2Tz MXene dispersions, J. Colloid Interface Sci. 605 (2022) 120–128, https://doi.org/https://doi-org.egateway.vit.ac.in/10.1016/j.jcis.2021.07.068.
[36] D. Soltman, B. Smith, S.J.S. Morris, V. Subramanian, Inkjet printing of precisely defined features using contact-angle hysteresis, J. Colloid Interface Sci. 400 (2013) 135–139, https://doi.org/https://doi-org.egateway.vit.ac.in/10.1016/j.jcis.2013.03.006.
[37] M. Orrill, D. Abele, M. Wagner, S. LeBlanc, Ink synthesis and inkjet printing of electrostatically stabilized multilayer graphene nanoshells, J. Colloid Interface Sci. 566 (2020) 454–462, https://doi.org/https://doi-org.egateway.vit.ac.in/10.1016/j.jcis.2020.01.095.
[38] H.C. Nallan, J.A. Sadie, R. Kitsomboonloha, S.K. Volkman, V. Subramanian, Systematic design of jettable nanoparticle-based inkjet inks: Rheology, acoustics, and jettability, Langmuir 30 (2014) 13470–13477, https://doi.org/10.1021/la502903y.
[39] L. Nayak, S. Mohanty, S.K. Nayak, A. Ramadoss, A review on inkjet printing of nanoparticle inks for flexible electronics, J. Mater. Chem. C 7 (2019) 8771–8795, https://doi.org/10.1039/C9TC01630A.
[40] M. Shariq, P. Majerič, B. Friedrich, B. Budic, D. Jenko, A.R. Dixit, R. Rudolf, Application of Gold(III) acetate as a new precursor for the synthesis of gold nanoparticles in PEG through ultrasonic spray pyrolysis, J. Clust. Sci. 28 (2017) 1647–1665, https://doi.org/10.1007/s10876-017-1178-0.
[41] M. Shariq, B. Friedrich, B. Budic, N. Hodnik, F. Ruiz-Zepeda, P. Majerič, R. Rudolf, Successful synthesis of gold nanoparticles through ultrasonic spray pyrolysis from a gold(III) nitrate precursor and their interaction with a high electron beam, ChemistryOpen 7 (2018) 533–542, https://doi.org/10.1002/open.201800101.
[42] S. Pandiyan, A. El-Kharouf, R. Steinberger-Wilckens, Formulation of spinel based inkjet inks for protective layer coatings in SOFC interconnects, J. Colloid Interface Sci. 579 (2020) 82–95, https://doi.org/https://doi-org.egateway.vit.ac.in/10.1016/j.jcis.2020.06.032.
[43] M. Shariq, S. Chattopadhyaya, R. Rudolf, A. Rai Dixit, Characterization of AuNPs based ink for inkjet printing of low cost paper based sensors, Mater. Lett. 264 (2020), 127332 https://doi.org/https://doi.org/10.1016/j.matlet.2020.127332.
[44] P. Majerič, D. Jenko, B. Friedrich, R. Rudolf, Formation mechanisms for gold nanoparticles in a redesigned ultrasonic spray pyrolysis, Adv. Powder Technol. 28 (2017) 876–883, https://doi.org/10.1016/j.apt.2016.12.013.
[45] F. Almyahi, T.R. Andersen, N.A. Cooling, N.P. Holmes, M.J. Griffith, K. Feron, X. Zhou, W.J. Belcher, P.C. Dastoor, Optimisation of purification techniques for the preparation of large-volume aqueous solar nanoparticle inks for organic photovoltaics, Beilstein J. Nanotechnol. 9 (2018) 649–659, https://doi.org/10.3762/bjnano.9.60.
[46] Dimatix, Materials Printer Jettable Fluid Formulation Guidelines, (2013) 95050.
[47] Y. Liu, B. Derby, Experimental study of the parameters for stable drop-on-demand inkjet performance, Phys. Fluids 31 (2019) 32004, https://doi.org/10.1063/1.5085868.
[48] R.K. Gangwar, V.A. Dhumale, D. Kumari, U.T. Nakate, S.W. Gosavi, R.B. Sharma, S. N. Kale, S. Datar, Conjugation of curcumin with PVP capped gold nanoparticles for improving bioavailability, Mater. Sci. Eng.: C 32 (2012) 2659–2663, https://doi.org/10.1016/j.msec.2012.07.022.
[49] D.P. Siregar, J.G.M. Kuerten, C.W.M. van der Geld, Numerical simulation of the drying of inkjet-printed droplets, J. Colloid Interface Sci. 392 (2013) 388–395, https://doi.org/https://doi-org.egateway.vit.ac.in/10.1016/j.jcis.2012.09.063.
[50] L. Spagnuolo, R. D'Orsi, A. Operamolla, Nanocellulose for paper and textile coating: the importance of surface chemistry, Chempluschem 87 (2022), e202200204, https://doi.org/10.1002/cplu.202200204.
[51] T. Öhlund, J. Örtegren, S. Forsberg, H.-E. Nilsson, Paper surfaces for metal nanoparticle inkjet printing, Appl. Surf. Sci. 259 (2012) 731–739, https://doi.org/10.1016/j.apsusc.2012.07.112.
[52] O. Shavdina, C. Grillot, A. Stolz, F. Giovannelli, V. Bertagna, J. Nicolle, C. Vautrin-Ul, C. Boulmer-Leborgne, N. Semmar, Effect of ink formulation on the inkjet printing process of Al–ZnO nanoparticles, J. Coat. Technol. Res. 18 (2021) 591–600, https://doi.org/10.1007/s11998-020-00427-z.
[53] S.(김 산) Kim, J.H.(최준혁) Choi, D.K.(손동기) Sohn, H.S.(고한서) Ko, Printability of inkjet according to supply pressure, Physics of Fluids. 35 (2023) 053304. https://doi.org/10.1063/5.0145985.
[54] Y. Huang, L. Jiang, B. Li, P. Premaratne, S. Jiang, H. Qin, Study effects of particle size in metal nanoink for electrohydrodynamic inkjet printing through analysis of droplet impact behaviors, J. Manuf. Process 56 (2020) 1270–1276, https://doi.org/10.1016/j.jmapro.2020.04.021.
[55] G.F. Trindade, F. Wang, J. Im, Y. He, A. Balogh, D. Scurr, I. Gilmore, M. Tiddia, E. Saleh, D. Pervan, L. Turyanska, C.J. Tuck, R. Wildman, R. Hague, C.J. Roberts, Residual polymer stabiliser causes anisotropic electrical conductivity during inkjet printing of metal nanoparticles, Commun. Mater. 2 (2021), 47, https://doi.org/10.1038/s43246-021-00151-0.